RADIO SCIENCE, VOL. 45, RS4005, doi:10.1029/2009RS004272, 2010

Effects of clock frequency stability on digital microwave radiometer performance

Jinzheng Peng[1] and Christopher S. Ruf[1]

Received 4 September 2009; revised 18 December 2009; accepted 15 March 2010; published 10 July 2010.

[1] A new generation of digital microwave radiometer back ends replaces conventional analog square-law detectors with a high-speed digital signal processing (DSP) stage to enhance their performance. The enhancements can include frequency subbanding for improved spectral resolution and mitigation of radio frequency interference, complex cross-correlation of orthogonally polarized signals for full Stokes polarimetry, and high-order moment (kurtosis) detection for improved radio frequency interference detectability. In each of these cases, the quality of the performance enhancement can be degraded by the nonideal realization of the desired DSP algorithm. In particular, instability in the master clock, which times the cadence of the DSP stage, can affect the performance. Analytical expressions are developed to model critical radiometer performance criteria as functions of the clock frequency stability. Experimental results are presented to validate the expressions. These results can be used to derive clock frequency stability requirements for future digital microwave radiometers.

Citation: Peng, J., and C. S. Ruf (2010), Effects of clock frequency stability on digital microwave radiometer performance, *Radio Sci.*, *45*, RS4005, doi:10.1029/2009RS004272.

1. Introduction

[2] Clocks perform a vital function in complex digital systems. They pace all digital signal processing (DSP) functions, including the initial sampling of the analog signal. The quality of a clock can be described by its frequency stability, which refers to its ability to maintain a constant frequency. Frequency instability is usually induced by thermal and shot noise, mechanical vibration, and temperature-dependent parasitic reactances [*Gonzalez*, 2007]. It can be periodic, random, or a mixture of the two. Periodic variations in clock frequency can cause harmonics and spurs in the output spectrum, whereas random variations raise the noise floor and broaden the desired spectral line. Either source of instability can result in serious performance degradation from intermodulation distortion and logic timing errors [*McCorquodale et al.*, 2003; *Reinhardt*, 2005]. Therefore, clock frequency stability can be an important parameter for determining the performance of digital systems. General expressions that relate clock stability to particular performance metrics of DSP functions that are performed in radiometry are developed here. These expressions can be used to determine the level of clock stability needed to meet particular DSP performance requirements. This can be especially useful in spaceflight and other low-power applications. Increased clock stability often comes at the price of higher power, e.g., by more tightly controlling oscillator temperature or by phase locking one oscillator to another, more stable, master clock. The expressions developed here will help to determine the minimum clock stability, and hence the lowest power, needed to meet particular DSP requirements.

[3] Conventional microwave radiometer receivers typically consist of an analog front end stage, which amplifies the antenna or calibration signal and sometimes downconverts it to a lower carrier frequency, followed by an analog back end stage, which rectifies and averages the signal using a square-law detector diode and video amplifier/low-pass filter [*Skou and Le Vine*, 2006]. The detected video signal is then digitized. A digital radiometer replaces the analog back end stage with a high-speed digitizer (typically clocked faster than twice the predetection bandwidth of the radiometer signal), followed by a DSP module. The DSP module can be either a field-programmable gate array (FPGA) or an applica-

[1]Space Physics Research Laboratory, Atmospheric, Oceanic and Space Sciences, University of Michigan, Ann Arbor, Michigan, USA.

0048-6604/10/2009RS004272

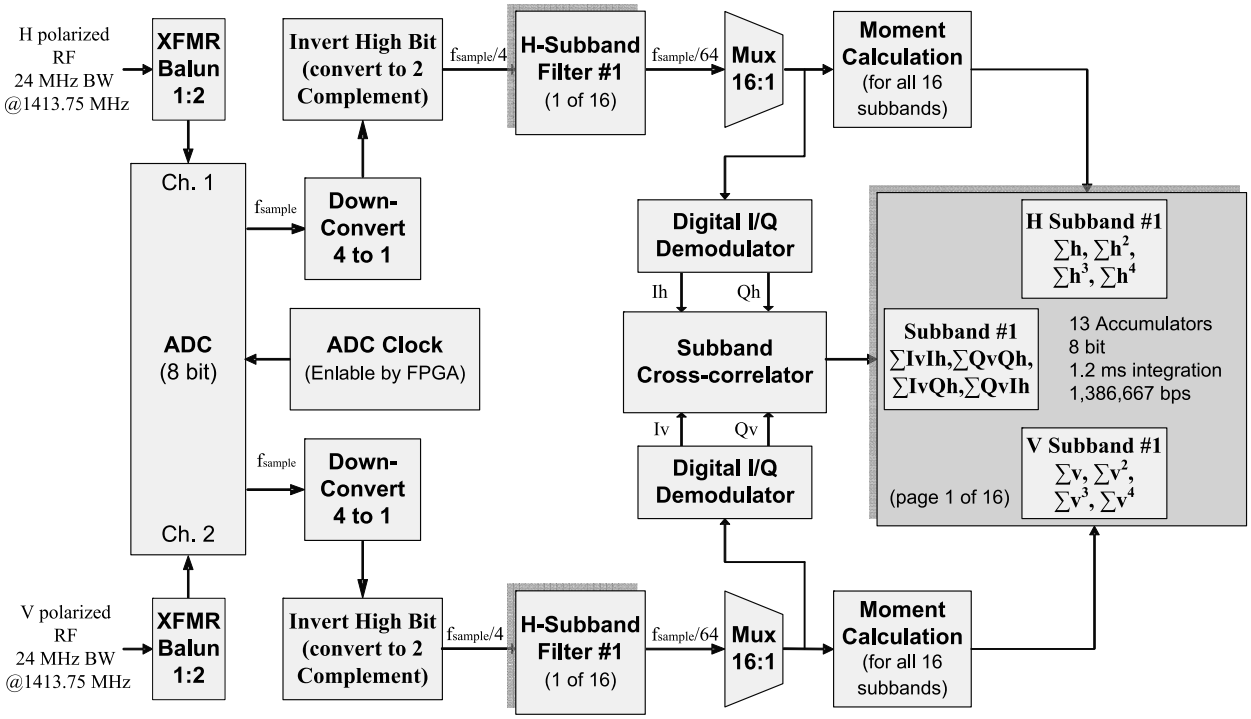

Figure 1. Radiometer digital back end signal processing flow.

tion-specific integrated circuit, depending on the speed and power requirements of a particular radiometer.

[4] A number of microwave radiometers with digital back ends have been built previously. Fully polarimetric capabilities were added to a dual-linear polarized conventional radiometer by digitally cross correlating the individual v- and h-pol signals [*Piepmeier and Gasiewski*, 2001]. The need for an analog frequency down-conversion stage was eliminated by digitizing a radiometer's RF signal at a subsampled clock rate and using the resulting aliasing as a digital mixer [*Fischman*, 2001]. The detection of low-level radio frequency interference (RFI) was enabled by a digital high-order moment detector (kurtosis detector), and the RFI was then mitigated by digital subband filters [*Ruf et al.*, 2006]. All of these features have recently been combined into a single-radiometer digital back end module. The module, which is described in greater detail in the following section, was developed as a proof-of-concept design for a possible spaceborne digital microwave radiometer. Its specific DSP algorithm is used as the basis for the performance analysis results presented in section 3. The module itself was also used, together with a custom clock that is capable of operating with a variable and controlled level of instability, in a series of tests intended to demonstrate experimentally the effects of clock instability. Those results are presented in section 4.

2. Description of Radiometer Digital Back End Module

[5] The digital back end module is a two-channel digitizer and signal processor designed for use by an L-band microwave radiometer. It uses commercial components, for all of which space-qualified equivalents are available. Two (v- and h-pol) analog input signals are digitized by a two-channel 8-bit analog-to-digital converter (ADC) chip (National Semiconductor ADC08D1000). The digitized signals are processed by a single Virtex II FPGA, which performs all critical DSP functions. Figure 1 shows an overview of the data path and processing inside the FPGA.

[6] The analog signals entering the ADC are filtered by the analog front end of the radiometer to lie between 1401.75 and 1425.75 MHz. The digitizing rate, f_s in Figure 1, is 279.26 MHz. Immediately following the ADC, the data rate is decimated by 4 to reduce the calculation load on later stages while still meeting the Nyquist sampling criterion. The high original sample frequency is necessary because the minimum clock frequency of this

ADC is 200 MHz. Note that the sample frequency is still well below the Nyquist rate dictated by the 1425.75-MHz highest-frequency component of the signal; subsampling the signal in this way effectively mixes it down from 1413.75 to ~34.9 MHz by controlled aliasing. It should be noted that successful subsampling in this manner requires that the analog input bandwidth of the ADC must be at least as wide as the highest-frequency component of the signal to be digitized.

[7] The DSP-intensive core of the FPGA begins with two separate but identical sets of subband filter banks, one set for each of the two polarization channels. Each filter bank consists of 16 separate but equidistant subband filters with equal 3-dB bandwidths of 1.5 MHz. Their outputs are decimated (subsampled) by a factor of 16 to further reduce the data rate of signals exiting each subband. The output data rate of each subband filter is 4.36 MS/s, which is well above their 3.0-MHz Nyquist rate.

[8] The data from each subband filter are fed into digital I/Q demodulators. The quadrature (Q) component is produced by passing the input signal through a finite impulse response (FIR) filter implementation of the Hilbert transform, while the in-phase (I) component is simply a time-delayed version of the input signal delayed by an appropriate amount to stay synchronized with the Q output. An ideal Hilbert transform provides a phase shift of +90° for positive frequencies and −90° for negative frequencies. It accepts a single real-valued input signal and produces a complex (I, Q) output signal. The complex version of the Nyquist sampling theorem states that each of the I and Q signals can be sampled at a frequency that is equal to the bandwidth of the real-valued input signal without loss of information (as opposed to sampling the input signal itself at twice its bandwidth). For this reason, the I and Q signals are decimated by a factor of 2 without loss of information. This helps reduce the data rate of subsequent DSP stages. The complex correlation between the v- and h-pol signals in each subband is computed by multiplying all possible pairs of I and Q components of one polarization with those of the other. The products are then averaged (accumulated) for an integration period.

[9] In parallel with the Hilbert transform filters, the data from each subband filter are also fed into moment calculators. The first, second, third, and fourth moments of the digitized data are computed by raising the signal to each of these powers and then averaging (accumulating) for an integration period. The second moment is essentially a digital version of the analog square-law detector used in conventional microwave radiometers. The lowest four moments can be combined together to compute the kurtosis of the signal, with which the presence of low-level RFI can be detected.

3. Theoretical Models for the Impact of Clock Noise

3.1. Clock Noise Model

[10] The output of an ideal clock can be expressed as a sine wave with constant amplitude, carrier frequency, and phase reference. Its spectrum is an impulse at the carrier frequency. For a practical (nonideal) clock, the output is more generally given by [*Hajimiri and Lee*, 1999]

$$v(t) = V_0[1 + n(t)]\cos[2\pi f_0 t + \theta(t)] \tag{1}$$

where V_0 is the maximum voltage swing, $n(t)$ is amplitude fluctuation, f_0 is the center frequency, and $\theta(t)$ is the phase fluctuation of the signal. V_0 and f_0 represent the shape of the ideal clock output waveform. The spectrum of a practical clock has sidebands close to the center frequency, f_0, and to its harmonics. The sidebands are generally referred to as *phase noise* in the frequency domain.

[11] Because of amplitude-limiting effects, the amplitude noise in an oscillator output is significantly reduced and can generally be ignored [*Hajimiri and Lee*, 1999]. Furthermore, because phase fluctuations can produce a random frequency, which is the derivative of the random phase fluctuation with respect to time, the phase fluctuation $\theta(t)$ can instead be represented by a frequency modulated component, or

$$v(t) = V_0 \cos\left[2\pi f_0 t + 2\pi f_\Delta \int_0^t x(\tau)\mathrm{d}\tau\right] \tag{2}$$

where f_Δ represents the maximum frequency shift away from f_0 in one direction and $x(t)$ is the frequency modulating signal. Equation (2) assumes that $x(t)$ is limited to the range ±1. The signal $x(t)$ is usually a random signal and represents frequency modulation noise in the oscillator. However, it might also contain a deterministic component. For example, an unwanted nonrandom signal might leak into an oscillator circuit or a signal might be added intentionally. In this article, we intentionally introduce sinusoidal frequency modulation signals, $x(t)$, into a modified clock circuit to investigate their effect on digital radiometer performance.

[12] Using the clock model described by equation (2), the clock frequency stability can be defined as

$$\delta_f = \frac{\sqrt{\langle x^2(\tau)\rangle} f_\Delta}{f_0} \tag{3}$$

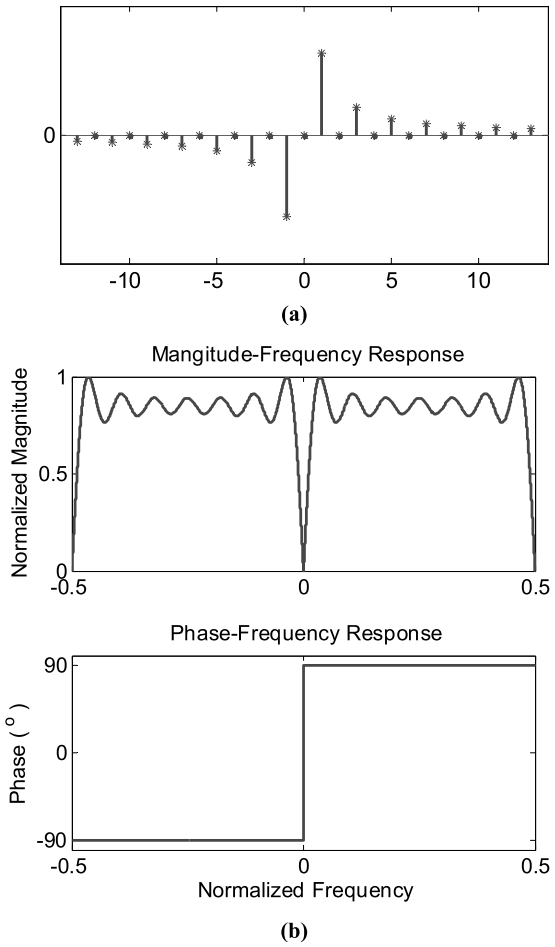

Figure 2. (a) Impulse response and (b) frequency response of the 27-tap Hilbert transform filter used in the digital radiometer back end.

where $\langle\cdot\rangle$ denotes expectation in the case of a random signal and the average over one period in the case of a sinusoidal signal.

3.2. Linear Tap Delay Line Filter Response to Clock Noise

[13] The digital back end includes a bank of FIR filters that divide the complete signal bandwidth into narrow subbands. Each of the subband filters can be represented as [*Oppenheim et al.*, 1983]

$$H(z) = \sum_{n=0}^{N} b_n z^{-n} \tag{4a}$$

and its Fourier transform is

$$H\left(e^{j\Omega}\right) = \sum_{n=0}^{N} b_n e^{-jn\Omega} \tag{4b}$$

where $\{b_n \mid n = 0, 1, \ldots, N\}$ is the set of the filter coefficients and Ω is the normalized frequency. Each individual subband filter has its own set of coefficients.

[14] Instability in the clock frequency can cause variations in the sample frequency, the bandwidth, and the center frequency of the subband filters. It results in a band-pass filter "shaking" in the frequency domain. A signal in the rejection region of a filter will have more chance to enter the passband of the filter. The degree of leakage will depend on the statistical distribution of the clock frequency.

[15] To simplify the analysis, we normalize the frequency of the input signal to that of the sample frequency. For example, for a sinusoidal input signal with frequency f, its normalized frequency after down-sampling will be

$$\begin{aligned} \Omega &= \frac{f}{f_s/4} - N \\ &= \frac{4f}{f_{ck}} - N \\ &= \frac{4f}{f_{ck,0} + f_d} - N \end{aligned} \tag{5}$$

where N is the down-sampling factor, $f_{ck,0}$ is the nominal clock frequency, and f_d is the frequency deviation of the clock. For the digital back end module considered here, $N = 20$. The instantaneous clock frequency is referred to as $f_{ck,m}$, and the instantaneous frequency deviation is $f_{d,m}$ ($= f_{ck,m} - f_{d,m}$). The frequency response of the subband filter stage, including the effects of instantaneous changes in clock frequency, will be given by

$$\begin{aligned} H(e^{j\Omega_m}) &= \sum_{n=0}^{N} b_n \exp\{-jn\Omega_m\} \\ &= \sum_{n=0}^{N} b_n \exp\left\{-jn\left(\frac{4f}{f_{ck,0} + f_{d,m}} - N\right)\right\} \end{aligned} \tag{6}$$

The output power of the subband FIR filter is determined as the expected value of the filter response, weighted with respect to the probability distribution of the clock frequency deviation. The final expression is given by

$$\begin{aligned} P_{tj}(f) &= \int \left|H\left(e^{j\Omega_m}\right)\right|^2 p(f_d)\mathrm{d}f_d \\ &= \int \left|\sum_{n=0}^{N} b_n \exp\left\{-jn\left(\frac{4f}{f_{ck,0} + f_d} - N\right)\right\}\right|^2 p(f_d)\mathrm{d}f_d \end{aligned} \tag{7}$$

The solution to equation (7) can be obtained numerically. Using this approach, the out-of-band rejection of the subband filter can be characterized if the statistical distribution of the clock frequency is known.

3.3. Complex Correlation Response to Clock Noise

[16] An ADC is a device that converts continuous signals to discrete digitals at a rate set by its clock, and it can be treated as a mixer in analog circuits except that the output of the ADC is discrete. The spectrum of the continuous signal differs from that of discrete samples in that the discrete sample spectrum is periodic with a frequency f_s, the sample frequency. If the ADC clock is not stable, the spectrum of the ADC output is broadened, and aliasing is induced. The width of the spectrum and aliasing increases with increased instability of the ADC clock.

[17] The band-pass filters in each subband are flat in magnitude and linear in phase. Therefore, they will not change the correlation coefficient of the signals if the signals are within the passband. The output of the band-pass filter is split into two paths. One path is simply delayed and is used as the real part of the signal, whereas the other is passed through a Hilbert transform filter to form the imaginary part of the signal. The impulse response corresponding to an ideal Hilbert transform filter in the frequency domain is odd-symmetric, and it has interleaved zeros. Because there is a step function in the frequency domain at DC, the impulse response in the time domain is infinite. When realized in practice, the impulse response must be truncated to a finite length. For example, the digital radiometer considered here uses is a 27-tap approximation. Its impulse response is shown in Figure 2a and its frequency response is shown in Figure 2b.

[18] As Figure 2b shows, the phase response of the truncated Hilbert transform filter is ideal, but its magnitude response is rippled in the frequency domain. It is this ripple that can cause magnitude imbalances between the in-phase and quadrature components of the signal when the clock is not stable. Variations in the magnitude imbalance, due to clock noise, can lead to the changes in the complex correlation.

[19] The impact of clock noise on the complex correlation can be assessed by considering the case of a sinusoidal radiometer input signal. Assume the input signal to the radiometer digital back end is sinusoidal with frequency, f, and phase angle, φ, between the v- and h-pol inputs. The I and Q filter outputs represent the real and imaginary components, respectively, of the complex signals to be correlated. They can be expressed as

$$\xi = \cos(2\pi ft) + j|H(f)|F\sin(2\pi ft) \tag{8a}$$

$$\eta = \cos(2\pi ft + \varphi) + j|H(f)|F\sin(2\pi ft + \varphi) \tag{8b}$$

where ξ and η are the complex signals in the v- and h-pol channels, F is a scale factor representing the amplitude balance (or gain balance) between I and Q filters ($F = 1$ with an ideal Hilbert transform filter), and it is the ratio of the I channel gain to the Q channel gain. In the plots of theoretical prediction shown later, the value of F is calculated assuming a stable clock. The function $H(f)$ is the frequency response of the Hilbert transform filter. After leaving the I and Q filters, the complex signals are cross-correlated (i.e., multiplied and averaged). The normalized complex correlation coefficient between the v- and h-pol signals is given by

$$\begin{aligned}\rho &= \frac{\left\langle \xi\eta^* \right\rangle}{\sqrt{\left\langle \xi\xi^* \right\rangle}\cdot\sqrt{\left\langle \eta\eta^* \right\rangle}} \\ &= \cos(\varphi) - j\frac{2\langle|H(\Omega)|\rangle F}{1+\left\langle |H(\Omega)|^2 \right\rangle F^2}\sin(\varphi)\end{aligned} \tag{9}$$

where $\langle\cdot\rangle$ denotes a time average and Ω, the normalized frequency after down-sampling, is given by equation (5).

[20] If the magnitude of the frequency response of the Hilbert transform filter is ideal, or flat, the product of $\langle|H(f)|\rangle$ and the scale factor F will be 1 and equation (9) reduces to

$$\rho = \cos(\varphi) - j\sin(\varphi) \tag{10}$$

In this case, the phase of the complex correlation coefficient is φ and the magnitude is unity, independent of φ. On the other hand, if the Hilbert transform filter is not ideal and the magnitude of its frequency response is not constant versus frequency, then the factor $\langle|H(\Omega)|\rangle F$ will not equal 1 and will vary with frequency. In this case, we have (see Appendix for proof)

$$\frac{2\langle|H(\Omega)|\rangle F}{1+\left\langle |H(\Omega)|^2 \right\rangle F^2} \neq 1 \tag{11}$$

If the inequality in equation (11) holds, then a more general expression for the magnitude and phase of the complex correlation coefficient is given by

$$|\rho| = \sqrt{\cos^2(\varphi) + \left[\frac{2\langle|H(\Omega)|\rangle F}{1+\left\langle |H(\Omega)|^2 \right\rangle F^2}\right]^2 \sin^2(\varphi)} \tag{12a}$$

$$\angle\rho = -\arctan\left\{\frac{2\langle|H(\Omega)|\rangle F}{1+\left\langle |H(\Omega)|^2 \right\rangle F^2}\tan(\varphi)\right\} \tag{12b}$$

Comparing equations (10) and (12), the change of the complex correlation coefficient is given by

$$\Delta_{|\rho|} = \sqrt{\cos^2(\varphi) + C^2 \sin^2(\varphi)} - 1 \tag{13a}$$

$$\Delta_{\angle\rho} = -\arctan\{C \tan(\varphi)\} + \varphi \tag{13b}$$

where C is a factor given by

$$C = \frac{2\langle|H(\Omega)|\rangle F}{1 + \left\langle |H(\Omega)|^2 \right\rangle F^2} \tag{14}$$

The sensitivity to clock noise of the errors in magnitude and phase of the complex correlation coefficient will vary, depending on the phase angle itself. This can be seen by examining the derivative of equation (13) with respect to phase angle. Maximum sensitivity to noise occurs when the phase angle satisfies

$$\sin\left(2\varphi_{\mathrm{p,mag}}\right) = 0 \quad \text{and} \quad \sin\left(2\varphi_{\mathrm{p,mag}}\right) \neq 0 \tag{15a}$$

$$\sin^2\left(\varphi_{\mathrm{p,pha}}\right) = \frac{1}{1 + C} \tag{15b}$$

where $\varphi_{\mathrm{p,mag}}$ is the phase angle at which the magnitude of the complex correlation coefficient is most sensitive to clock noise and $\varphi_{\mathrm{p,pha}}$ is the phase angle at which the phase of the complex correlation coefficient is most sensitive. Over the range [−180, 180], the solution for $\varphi_{\mathrm{p,mag}}$ is ±90°. For $\varphi_{\mathrm{p,pha}}$, there are four solutions, given by

$$\begin{aligned} \varphi_{\mathrm{p,pha}} &= \pm \arcsin\left(\frac{1}{\sqrt{1 + C}}\right) \quad \text{and} \\ \varphi_{\mathrm{p,pha}} &= \pm\left[\arcsin\left(\frac{1}{\sqrt{1 + C}}\right) + 90^\circ\right] \end{aligned} \tag{16}$$

Assuming the clock frequency instability is not serious, C will be close to 1, and the solutions for $\varphi_{\mathrm{p,pha}}$ are ±45° and ±135°.

[21] To illustrate the effect of clock frequency instability on the correlation measurements, two numerical examples are considered. The first example assumes that the clock frequency is varied sinusoidally; the second example assumes that the clock frequency is varied in a random Gaussian manner. The correlation coefficient magnitude and phase variations with clock frequency instability are shown in Figure 3. From these plots, it can be seen that the sensitivity of the correlation coefficient is indeed related to the phase angle of the correlation. If the input phase angle is equal to 0° or 180°, the sensitivity is 0; otherwise, the correlation coefficient magnitude has the highest sensitivity at input phase angle 90° (also at −90°; not shown in Figure 3), whereas the correlation coefficient phase has the highest sensitivity near 45° and 135° (also at −45° and −135°; not shown here).

[22] Note that, with sinusoidal perturbations in clock frequency, the sensitivity of the correlation coefficient has two local maxima as the RMS clock instability is increased, whereas with random Gaussian perturbations the sensitivity grows monotonically with RMS clock noise. This is due to the distribution of the clock frequency in the sinusoidal case. In both cases, however, the phase angles at which sensitivity to noise is maximum are the same and are as predicted by equations (15) and (16).

4. Experimental Validation

[23] A test system was developed to evaluate the sensitivity of the digital radiometer back end to clock frequency instability. An HP 8656B signal generator served as the clock; its capability for modulation can be used to generate controlled levels and types of clock noise. Sinusoidal clock instability is generated using the internal 1-kHz modulation option of the signal generator. Random Gaussian clock instability is generated using the signal generator's external modulation option. In this case, the external modulation signal is supplied by an arbitrary waveform generator programmed to produce band-limited white Gaussian noise. For both modulation signals, the maximum frequency deviation value (f_Δ in equation (1)) can be varied to change the RMS level of the clock frequency instability.

[24] A second signal generator is used to produce a sine wave as the radiometer input signal. Its frequency is centered on 1 of the 16 subbands of the digital radiometer. The sine wave is split into two paths by a power divider to form the v- and h-pol input signals. The RF cables connecting the power divider to the radiometer have equal lengths so that the v- and h-pol signals are in-phase. Tests were also performed with varying relative lengths of the two RF cables to verify the sensitivity dependence on the input phase angle of the signals.

4.1. Out-of-Band Rejection Sensitivity to Clock Noise

[25] The out-of-band rejection of the digital band-pass filters was tested using as an input signal a sinusoid positioned 1.5 MHz from the center of the filter (which also has a 1.5-MHz 3-dB bandwidth). Nominal out-of-band rejection, relative to the response at band center, is approximately 24 dB when no intentional clock noise is added. Increasing levels of clock noise were then added,

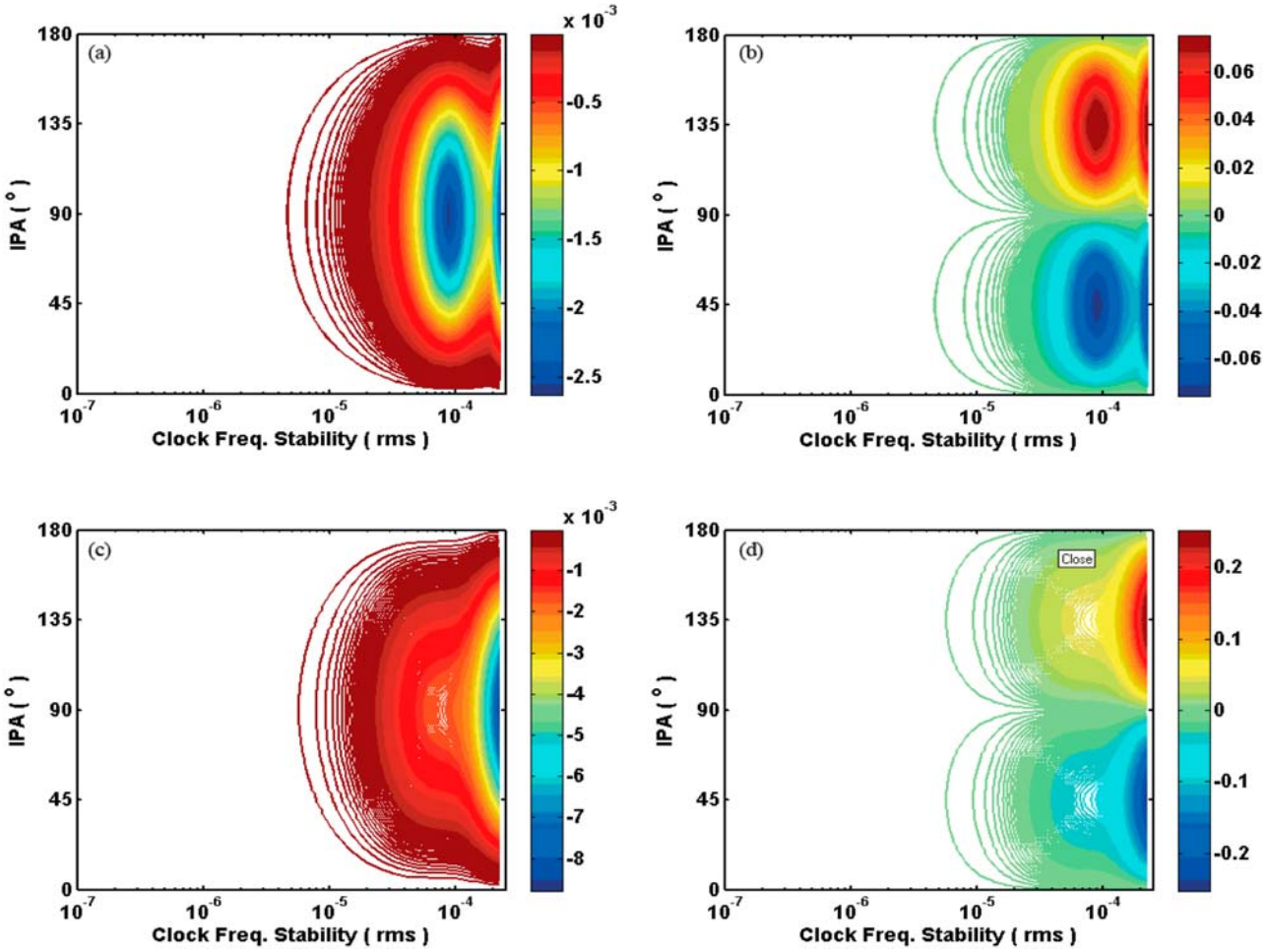

Figure 3. Variation of component of correlation coefficient with type of jitter: (a) magnitude with sinusoidal clock frequency, (b) phase with sinusoidal clock frequency, (c) magnitude with random clock frequency (Gaussian), and (d) phase with random clock frequency (Gaussian).

and the resulting out-of-band rejection was measured and compared with the theoretical predictions given by equation (12). The results are shown in Figure 4 for both sinusoidal and random Gaussian cases of clock modulation. In both cases, the degradation in out-of-band rejection is seen to grow with clock noise and to closely follow the theoretical predictions based on equation (12). Note, however, that there is a consistent offset between theory and measurements, with the measured filter performance consistently a little worse than predicted. This is likely due to the noise that is already present in the clock when no additional clock modulation has been added by us. The RMS clock frequency stability noted in Figure 4 only represents the noise due to our external modulation of the clock.

4.2. Correlation Coefficient Sensitivity to Clock Noise

[26] The magnitude and phase of the correlation coefficient measured by the digital complex correlator were tested using as input signals a pair of sinusoids positioned at the center of one of the band-pass filters' passbands. The relative phase of the two sinusoids (entering the v- and h-pol channels of the radiometer) was set to 10°, 51°, and 96° by varying RF cable lengths between the signal source and the radiometer. Increasing levels of clock noise were then added, and the measured changes in magnitude and phase of the complex correlation coefficient were compared with the theoretical predictions given by equation (13). The results are shown in Figures 5 and 6 for the magnitude and phase, respectively. In each case, the

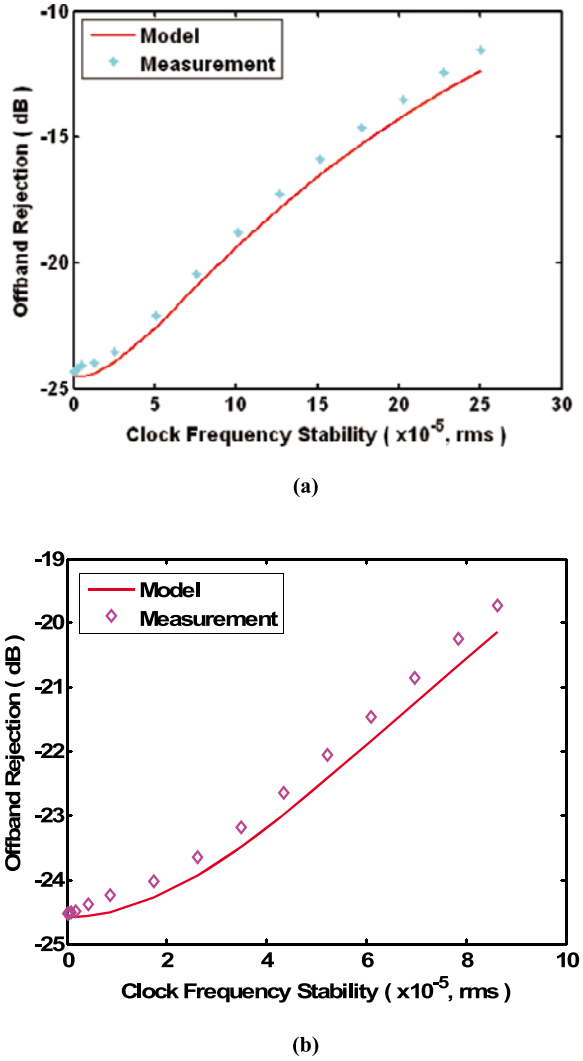

Figure 4. Out-of-band rejection of a digital band-pass filter with (a) sinusoidal and (b) random Gaussian clock noise.

change in correlation magnitude and phase grows with clock noise and closely follows the theoretical predictions. Note that the measured sensitivity to clock noise does depend strongly on the relative phase of the v- and h-pol input signals, as predicted by equation (13). Overall, the correlation magnitude is seen to be much more strongly affected by clock noise. The impact of clock noise on the correlation phase is sufficiently small (<0.05° for all cases considered here) that the 0.01° standard error in the phase measurements (because of the finite number of samples accumulated in each integration period) introduces noticeable scatter in the plots in Figure 6. Nonetheless, the correlation phase measurements do also confirm the dependence of sensitivity to noise on the phase of the input signals.

5. Conclusions

[27] Analytical expressions have been developed to relate several critical performance criteria of a microwave radiometer digital back end to the RMS instability of the

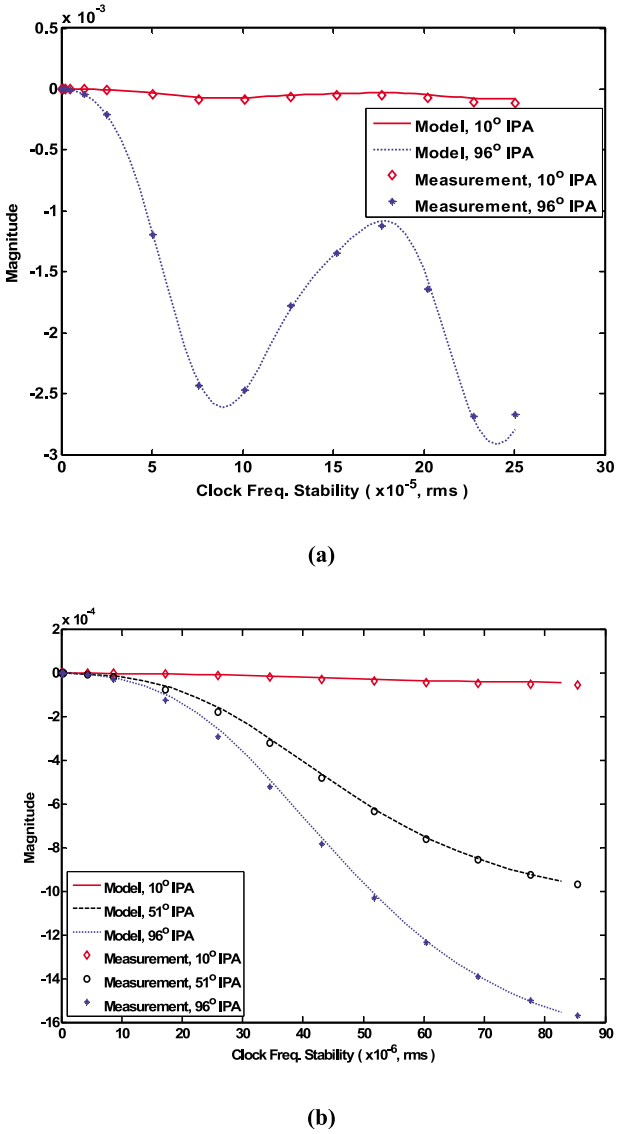

Figure 5. Variation of correlation coefficient of magnitude with (a) sinusoidal and (b) random Gaussian clock noise. The magnitude is largely insensitive to clock noise for input signal phase angles near 0° and has maximum sensitivity for input signal phase angle near 90°.

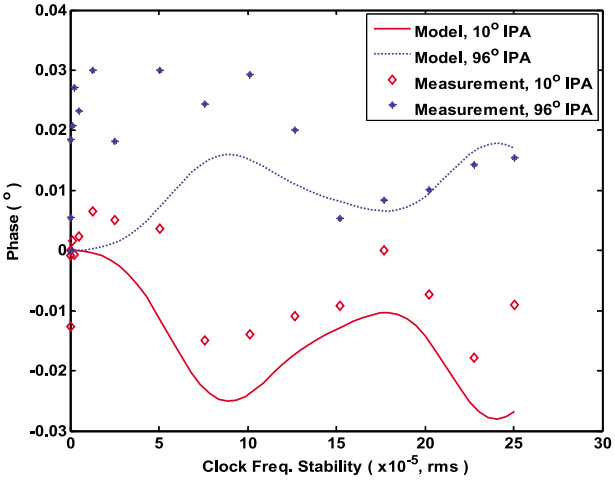

(a)

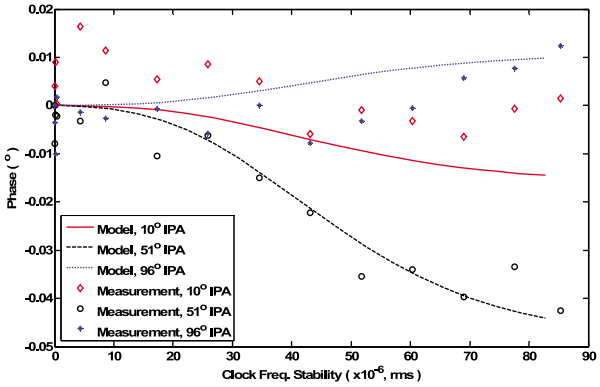

(b)

Figure 6. Variation of correlation coefficient phase with (a) sinusoidal and (b) random Gaussian clock noise. The phase is largely insensitive to clock noise for input signal phase angles near 0°and 90° and has maximum sensitivity for input signal phase angle near 45°. However, in all cases, the absolute magnitude of the phase error is quite small, measuring less than 0.05° for the worst case. Scatter in the measured correlation phase in the figure is due to measurement error, which had a standard deviation of 0.01°.

digital clock that times the signal processing operations performed. A general expression for the effect of clock noise on a linear-tap delay line filter is presented, and then the special case of a band-pass filter is considered. The out-of-band rejection of the filter is shown to degrade as the clock noise increases. Expressions are also developed for the change in magnitude and phase of a digital complex correlator as a function of the clock noise. The change is found to depend strongly on the phase of the correlation. For both the magnitude and phase, sensitivity to clock noise is smallest at phase angles of 0° and 180°. In the case of the magnitude, the sensitivity to noise is greatest at phase angles of −90° and 90°. In the case of the phase, the sensitivity to noise is greatest at phase angles of ±45° and ±135°.

[28] The analytical expressions relating clock noise to performance have been validated experimentally using an L-band digital radiometer with a digital clock that has been modified so that its noise level can be varied in a controlled way. Deterioration of the band-pass filter response and the complex correlation with clock noise level and, in the case of the complex correlation, with the correlation phase all closely match the theoretical predictions.

[29] The results presented here can be used as the basis for deriving stability requirements on the digital clock used in a digital microwave radiometer. A specific RMS stability requirement would follow from the performance requirements levied on the back end DSP stage of the radiometer. On the basis of the results presented here, with a particular digital radiometer design, an RMS clock stability of 10^{-5} or better is found to result in no significant degradation in performance. Designs with significantly higher clock rates or with significantly larger numbers of bits of quantization could be more sensitive to clock noise, so the general sensitivity expressions developed here should be re-evaluated for that particular design.

Appendix A

[30] Assume that the following equation holds, or

$$\frac{2\langle |H(\Omega)| \rangle F}{1 + \left\langle |H(\Omega)|^2 \right\rangle F^2} = 1 \tag{A1}$$

Because F is real and constant, it can be moved inside the operation $|\cdot|$. Then the above equation becomes

$$\left\langle |H(\Omega)F|^2 \right\rangle - 2\langle |H(\Omega)F| \rangle + 1 = 0 \tag{A2}$$

or

$$\left\langle [|H(\Omega)F| - 1]^2 \right\rangle = 0 \tag{A3}$$

The equation holds only if the following equation holds

$$|H(\Omega)F| = 1 \tag{A4}$$

Because F is real and constant, the magnitude of $H(\Omega)$ should be constant and will not be a function of Ω; otherwise, equation (A1) cannot be hold.

[31] **Acknowledgments.** The work reported here was supported in part by the NASA Goddard Space Flight Center and its Earth Science Technology Office under grants NNG05GB08G and NNG05GL97G.

References

Fischman, M. A. (2001), Development of a direct-sampling digital correlation radiometer for earth remote sensing applications, Ph.D. dissertation, Univ. of Michigan, Ann Arbor.

Gonzalez, G. (2007), *Foundations of Oscillator Circuit Design*, Arteck House, Boston, MA.

Hajimiri, A. and T. H. Lee (1999), *The Design of Low Noise Oscillator*, Kluwer Acad., Boston, MA.

McCorquodale, M. S., D. Mei Kim, and R. B. Brown (2003), Study and simulation of CMOS LC oscillator phase noise and jitter, in *Proceedings of the 2003 International Symposium on Circuits and Systems*, ISCAS '03.

Oppenheim, A. V., A. S. Willsky, and I. T. Young (1983), *Signals and Systems*, Prentice Hall, Englewood Cliffs, NJ.

Piepmeier, J. R., and A. J. Gasiewski (2001), Digital correlation microwave polarimetry: analysis and demonstration, *IEEE Trans. Geosci. Remote Sens.*, *39*(11), 2392–2410.

Reinhardt, V. S. (2005), A review of time jitter and digital systems, in *Proceedings of the 2005 IEEE International Frequency Control Symposium and Exposition*.

Ruf, C. S., S. M. Gross, and S. Misra (2006), RFI detection and mitigation for microwave radiometry with an agile digital detector, *IEEE Trans. Geosci. Remote Sens.*, *44*(3), 694.

Skou, N., and D. L. Vine, (2006), *Microwave Radiometer Systems: Design and Analysis*, Artech House, Boston, MA.

J. Peng and C. S. Ruf, Space Physics Research Laboratory, Atmospheric, Oceanic and Space Sciences, University of Michigan, 2455, Hayward St., Ann Arbor, MI 48109-2143, USA. (cruf@umich.edu)